

# Analysis of Micro-Doppler Signatures of Small UAVs Based on Doppler Spectrum

KI-BONG KANG 

JAE-HO CHOI 

Pohang University of Science and Technology Pohang, South Korea

BYUNG-LAE CHO 

JUNG-SOO LEE 

Agency for Defense Development Daejeon, South Korea

KYUNG-TAE KIM 

Pohang University of Science and Technology Pohang, South Korea

**Most of the investigations on the micro-Doppler (MD) effect caused by a small unmanned aerial vehicle (UAV) have been conducted using joint time-frequency (JTF) images rather than the Doppler spectrum. On the other hand, several researchers utilized the Doppler spectrum instead of JTF images to observe the MD signature of a small UAV, and found the relationship between the spectral distribution of a small UAV and its physical specifications. However, the studies using the Doppler spectrum still lack concrete and theoretical foundations of the MD effects of a small UAV, focusing mainly on phenomena identified by measurement data. In this article, we establish the theoretical foundation connecting the MD signatures and motion dynamics of small UAVs based on the Doppler spectrum, and analyze their spectral distribution using simulations and measured data. In addition, experimental analysis is conducted using the data measured from various types of small UAVs considering the translational motion and aspect change. In contrast to already existing investigations, we completely explain and predict the changes on the Doppler spectrum relative to the physical specifications of a small UAV (e.g., blade length and**

Manuscript received July 10, 2020; revised October 28, 2020 and March 16, 2021; released for publication March 21, 2021. Date of publication April 20, 2021; date of current version October 11, 2021.

DOI No. 10.1109/TAES.2021.3074208

Refereeing of this contribution was handled by Kyung-Tae Kim.

This work was supported in part by the Threat Target Modeling and Characterization Program of the Agency for Defense Development and in part by BK21 FOUR Program.

Authors' addresses: Ki-Bong Kang, Jae-Ho Choi, and Kyung-Ta Kim are with the Department of Electrical Engineering, Pohang University of Science and Technology Pohang 790-784, South Korea, E-mail: (kbb131@postech.ac.kr; jhchoi93@postech.ac.kr; kkt@postech.ac.kr); Byung-Lae Cho and Jung-Soo Lee are with DFH Satellite Company, Ltd. Beijing 100094, China, E-mail: (chobl@add.re.kr; jslee07@add.re.kr). (Corresponding author: Kyung-Tae Kim.)

0018-9251 © 2021 IEEE

rotor rotation rate). In particular, we show that the Doppler spectrum, compared to the JTF images, is a considerably simple and useful tool for analyzing the MD effects of small flying UAVs. The analysis results reveal that the MD features obtained from the measured echoes of small UAVs have considerable potential for detection and classification of small UAVs.

## I. INTRODUCTION

Small unmanned aerial vehicles (UAVs) have recently become easy to operate, readily available in the market, and affordable [1]. Small UAVs can be used for various purposes, such as aerial photography, agricultural activities, environmental monitoring, or leisure. Although the developments in the technology of small UAVs have generated many benefits, the misuse of these aircrafts in criminal and antisocial activities, including military threats, has also increased. Moreover, small UAVs may be dangerous when these are operated by beginners who may potentially lose control. Accordingly, the demand for small UAV detection techniques has significantly increased [2].

Radar are among the most effective tools for target detection because they are weather independent, capable of measuring distance and velocity [3]–[11]. However, it is difficult to detect real small flying UAVs because of their small radar cross-section (RCS) and low-altitude and low-speed flight [9], [12]–[15]. Although the transmitting power of radars is sufficiently high to detect small UAVs, distinguishing UAVs from birds is still difficult because they have similar moving speeds and RCSs [10], [16], [17]. Hence, a new method capable of differentiating small UAVs from birds is crucial [10], [11], [18].

The rotation of blades of a small UAV is referred to as micromotion. It can induce a periodic and time-varying frequency modulation of the returned signal. This periodic signal can produce a time-varying Doppler frequency shift called micro-Doppler (MD) effect. The characteristics of this MD effect are dependent on various factors, such as rotation rate, blade length, and number of blades, which can provide information on the dynamics and physical specifications of a small UAV with micromotion [19], [20]. Thus, the MD signatures caused by the small UAVs would be a useful information for detection and classification of small UAVs.

Most of the studies using the MD signatures for detecting small UAVs have been conducted based on the joint time-frequency (JTF) image, which is suitable for obtaining the information of the time-varying echo signal of a target. In [21]–[23], the JTF images are used as training/test data for classification of small UAVs based on deep learning. The methods in [24]–[26] utilized the JTF images to extract MD-based features for recognizing the type of small UAVs. In [27]–[30], The JTF image was transformed into cadence-velocity diagram [27], [28] or cepstrogram [29], [30], and they were employed to improve the classification performance of small UAVs. Recently, there were attempts to develop the detector/classifier using the helicopter rotor

modulation lines observed in the long time integrated JTF image [31]–[33].

As mentioned, many researchers have utilized the JTF image, and have verified that the JTF image is very useful to identify the MD signatures of small UAVs [34]–[36]. However, the JTF image is obtained by taking a number of Fourier transforms (FTs) in many windowed segments; hence, the techniques based on the JTF image is computationally expensive. In addition, it requires a huge amount of storage space for training database, especially when JTF images are used to classify small UAVs.

On the other hand, the Doppler spectrum can be easily obtained by performing a single FT. This Doppler spectrum provides spectral distribution caused by MD effect. Thus, the Doppler spectrum rather than the JTF image could be a useful tool to observe the MD signatures of small UAVs with rotating blades. The Doppler spectrum has been considered as a tool to analyze the MD signature, but few studies have been conducted using the Doppler spectrum for detection and classification of the small UAVs with rotating blades. Recently, in [37], the Doppler spectrum was used to estimate the physical specifications of small UAVs. In [38]–[42], researchers have examined that the MD effects of small UAVs can be identified by utilizing the Doppler spectrum, and they found that the characteristics of the spectral distribution of a small UAV are related to its physical specifications. However, existing studies have mainly focused on a simple investigation of the actual measurement data of small UAVs, and thereby, still lack concrete and theoretical foundations to formulate a relationship between the Doppler spectrum containing the MD effects and the physical specifications, associated with motion dynamics and physical dimension of a small UAV. Even though research has been conducted to demonstrate the characteristics of the MD signature of a rotating blade based on the Doppler spectrum [42]–[45], the MD signature for a small and moving UAV with multiple blades mounted on the multiple rotors cannot be fully explained.

In this article, we completely establish the theoretical foundation that links the MD signatures and physical specifications of small UAVs based on the Doppler spectrum, and thoroughly analyze their features acquired from the Doppler spectrum. In order to establish the theoretical foundation, we build a signal model in the time domain of a small flying UAV considering rotation rate of rotors, the length of a blade, the number of rotors, radial velocity, and aspect change. Subsequently, the spectral distribution of a received echoes in the frequency domain is theoretically analyzed. Based on this analysis in the frequency domain, the actual physical specifications and motion dynamics of a small UAV are compared with those obtained from the Doppler spectrum using simulations and measured data. In particular, the experimental analysis is performed using the measured data obtained from various types of small UAVs, considering the translational motion and aspect change. As a result, the changes in the MD signatures relative to the physical specifications of a small UAV (e.g., blade length and rotor rotation rate) are successfully explained and predicted

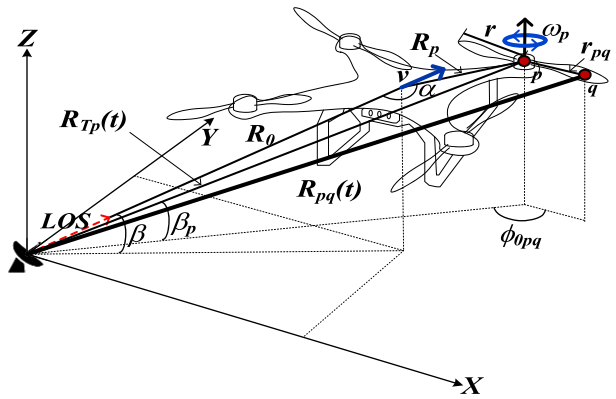


Fig. 1. Geometry of a small UAV in a dynamic state.

on the Doppler spectrum. Moreover, it is demonstrated that the Doppler spectrum, compared to JTF images, is a considerably simple and useful tool for investigating the MD signature of a small UAV. The analysis results indicate that the MD features obtained from the Doppler spectrum have considerable potential for detecting and classifying small UAVs.

The remainder of this article is organized as follows. In Section II, an echo signal model considering the rotating blades, radial velocity, and small UAV aspect change is introduced. The section also presents the dynamic analyses of MD effects and their relationship to the physical specifications of a small UAV. In Section III, the validation of theoretical investigations introduced in Section II is elaborated based on real measurement data using an X-band radar. Finally, Section IV concludes this article.

## II. ANALYSIS OF MD SIGNATURE OF A SMALL UAV

In this section, the relationship between the motion dynamics and MD features induced by the rotating blades of a small UAV are presented in detail. It is also demonstrated that these MD features provide useful information related to the physical specifications of a small UAV. The echo signal model is first derived to account for the dynamics of a small UAV with micromotion and translational motion. Thereafter, the MD features induced by the rotating blades in the frequency domain are analyzed.

### A. Signal Model of a Small Flying UAV in Time Domain

The geometry of a small flying UAV with its rotating blades is shown in Fig. 1. The radar is located at the origin  $(0, 0, 0)$  in  $XYZ$  coordinates,  $R_0$  is the distance between the radar and center of the small UAV along the radar line of site (LOS), and  $\beta$  is the angle between  $R_0$  and the  $XY$  plane. It is assumed that the coherent processing interval (CPI) is sufficiently short such that both the translational motion of its main body and micromotion of its blades can be modeled using only the constant radial velocity ( $v$ ) and constant angular velocity ( $\omega_p$ ), respectively;  $\omega_p$  is the angular velocity of the  $p$ th rotor. If  $R_p$  is the distance between the centers of the small UAV and the  $p$ th rotor, and  $\alpha$  is the angle between  $R_0$  and  $R_p$ , then the distance

between the radar and center of the  $p$ th rotor can be written as follows.

$$R_{Tp}(t) = \sqrt{(R_0 + vt)^2 + R_p^2 - 2(R_0 + vt)R_p \cos(\alpha)}. \quad (1)$$

For a target in the far field, i.e., for  $R_0 + vt \gg R_p$ , (1) can be approximated as

$$R_{Tp}(t) \approx R_0 + vt - R_p \cos(\alpha). \quad (2)$$

Only the radial motion of the small UAV changes  $R_{Tp}(t)$ . If the  $q$ th scatterer is on the blade of the  $p$ th rotor, the distance between the radar and the  $q$ th scatterer can be represented as (3) shown at bottom of this page, where  $r_{pq}$  is the distance between the center of the  $p$ th rotor and  $q$ th scatterer ( $r_{pq} \leq$  blade length,  $r$ ),  $\beta_p$  is the angle between  $R_{Tp}(t)$  and the XY plane or that between  $R_{Tp}(t)$  and the tip path plane (TPP), and  $\phi_{0pq}$  is an initial phase of the  $q$ th scatterer [46]. If  $R_{Tp}(t) \gg r_{pq}$ , then  $\beta_p \approx \beta$ , and Eq. (3) shown at bottom of this page, is approximately expressed as

$$R_{pq}(t) \approx R_{Tp}(t) - r_{pq} \cos(\beta) \cos(\omega_p t + \phi_{0pq}). \quad (4)$$

The second term in (4) is only changed by the micro-motion. Thus, the distance between the radar and the  $q$ th scatterer on the blade can be modeled as the linear sum of distances determined by the translational motion and micro-motion

$$R_{pq}(t) = R_{Tp}(t) + R_{Mpq}(t) \quad (5)$$

where

$$R_{Mpq}(t) = -r_{pq} \cos(\beta) \cos(\omega_p t + \phi_{0pq}). \quad (6)$$

The echo signal received from the small UAV can then be expressed in the time domain as

$$\begin{aligned} s(t) &= \sum_{k=1}^K A_k \exp \left\{ -j \frac{4\pi}{\lambda} R_{Tk}(t) \right\} \\ &+ \sum_{p=1}^P \sum_{q=1}^Q B_{pq} \exp \left\{ -j \frac{4\pi}{\lambda} (R_{Tp}(t) + R_{Mpq}(t)) \right\} \end{aligned} \quad (7)$$

where  $K$  is the number of scatterers on the body of a small UAV,  $A_k$  is the complex amplitude of the  $k$ th scatterer,  $P$  is the number of rotors,  $Q$  is the number of scatterers on the blades of each rotor, and  $B_{pq}$  is the complex amplitude of the  $q$ th scatterer on the  $p$ th rotor. Equation (7) can be further written as

$$\begin{aligned} s(t) &= \bar{A} \exp \left\{ -j \frac{4\pi}{\lambda} R_T(t) \right\} \\ &+ \sum_{p=1}^P \sum_{q=1}^Q \bar{B}_{pq} \exp \left\{ -j \frac{4\pi}{\lambda} (R_T(t) + R_{Mpq}(t)) \right\} \end{aligned} \quad (8)$$

where

$$\bar{A} = \sum_{k=1}^K A_k \exp \left[ -j \frac{4\pi}{\lambda} \{R_0 - R_k \cos(\alpha)\} \right] \quad (9)$$

$$\bar{B}_{pq} = B_{pq} \exp \left[ -j \frac{4\pi}{\lambda} \{R_0 - R_p \cos(\alpha)\} \right] \quad (10)$$

$$R_T(t) = vt. \quad (11)$$

Finally, (8) can be further simplified into

$$s(t) = \bar{A} s_T(t) + s_T(t) \times s_M(t) \quad (12)$$

where

$$s_T(t) = \exp \left\{ -j \frac{4\pi}{\lambda} R_T(t) \right\} = \exp \left\{ -j \frac{4\pi}{\lambda} vt \right\} \quad (13)$$

$$s_M(t) = \sum_{p=1}^P \sum_{q=1}^Q \bar{B}_{pq} s_{Mpq}(t) \quad (14)$$

$$\begin{aligned} s_{Mpq}(t) &= \exp \left\{ -j \frac{4\pi}{\lambda} R_{Mpq}(t) \right\} \\ &= \exp \{j\Gamma_{pq} \cos(\omega_p t + \phi_{0pq})\} \end{aligned} \quad (15)$$

$$\Gamma_{pq} = \frac{4\pi}{\lambda} r_{pq} \cos(\beta). \quad (16)$$

## B. Doppler Spectrum in Frequency Domain

The Doppler spectrum of a small UAV can be obtained by taking the FT of (12) with respect to  $t$

$$S(f) = \bar{A} S_T(f) + S_T(f) * S_M(f) \quad (17)$$

where  $*$  is the convolution operator, and  $S_T(f)$  is the Doppler spectrum of  $s_T(t)$  given as

$$S_T(f) = \delta \left( f + \frac{2v}{\lambda} \right). \quad (18)$$

In (15),  $s_{Mpq}(t)$  can be expressed using a Fourier series expansion as follows [45]:

$$\begin{aligned} s_{Mpq}(t) &= \sum_{m=-\infty}^{\infty} J_m(\Gamma_{pq}) \exp \left\{ jm \left( \phi_{0pq} - \frac{\pi}{2} \right) \right\} \exp(j\omega_p m t) \end{aligned} \quad (19)$$

where  $J_m()$  is the  $m$ th-order Bessel function of the first kind. The Doppler spectrum of  $s_{Mpq}(t)$  becomes

$$S_{Mpq}(f) = \sum_{m=-\infty}^{\infty} C_{pq}(m) \delta \left( f - \frac{\omega_p}{2\pi} m \right) \quad (20)$$

---


$$R_{pq}(t) = \{R_{Tp}(t)^2 + r_{pq}^2 - 2R_{Tp}(t) r_{pq} \cos(\beta_p) \cos(\omega_p t + \phi_{0pq})\}^{\frac{1}{2}} \quad (3)$$

where

$$C_{pq}(m) = J_m \left( \Gamma_{pq} \right) \exp \left\{ jm \left( \phi_{0pq} - \frac{\pi}{2} \right) \right\} \quad (21)$$

and  $\delta()$  is the Dirac delta function. Thereafter,  $S_M(f)$  can be obtained using (20)

$$S_M(f) = \sum_{p=1}^P \sum_{q=1}^Q \bar{B}_{pq} \sum_{m=-\infty}^{\infty} C_{pq}(m) \delta \left( f - \frac{\omega_p}{2\pi} m \right). \quad (22)$$

In (21),  $\phi_{0pq}$  is  $\phi_{0pq} = 2\pi n/N + \phi_p$  ( $n = 1, 2, \dots, N$ ), where  $N$  is the number of blades on each rotor, and  $\phi_p$  is an initial phase of the  $p$ th rotor. Therefore, (22) becomes approximately zero when  $m$  is not an integer multiple of  $N$  under the assumption that  $|\bar{B}_{p1}| \approx |\bar{B}_{p2}| \approx \dots \approx |\bar{B}_{pQ}|$

$$S_M(f) \approx \sum_{p=1}^P \sum_{q=1}^Q \sum_{m=-\infty}^{\infty} \bar{B}_{pq} C_{pq}(Nm) N \delta \left( f - \frac{\omega_p}{2\pi} Nm \right). \quad (23)$$

By substituting (18) and (23) into (17), the Doppler spectrum of a small UAV can be finally expressed as

$$\begin{aligned} S(f) &= \bar{A} \delta \left( f + \frac{2v}{\lambda} \right) \\ &+ \sum_{p=1}^P \sum_{q=1}^Q \sum_{m=-\infty}^{\infty} \bar{B}_{pq} C_{pq}(Nm) \delta \left( f + \frac{2v}{\lambda} - \frac{\omega_p}{2\pi} Nm \right). \end{aligned} \quad (24)$$

In (24), it is clear that the Doppler spectrum of a small UAV consists of pairs of harmonic spectral lines ( $\omega_p Nm / 2\pi$ ) around the center frequency,  $-2v/\lambda$ . The interval between adjacent spectral lines, usually called chopping frequency [44], is

$$\text{Chopping frequency} = \frac{N\omega_p}{2\pi}. \quad (25)$$

The spectral lines are distributed over the specific frequency band. For  $m > \Gamma_{pq}/N$ ,  $|J_m(0)|$  rapidly converges to zero [47]. Accordingly, using Carson's bandwidth rule, the frequency bandwidth becomes [45]

$$\begin{aligned} &[f_{d\min}, f_{d\max}] \\ &= \left[ -\frac{2}{\lambda} (r \cos(\beta) \omega_{\max} + v), \frac{2}{\lambda} (r \cos(\beta) \omega_{\max} - v) \right] \end{aligned} \quad (26)$$

where  $f_{d\min}$  is the minimum value of the Doppler spectrum,  $f_{d\max}$  is the maximum value given by (24),  $r$  is the blade length,  $\omega_{\max}$  is the maximum angular velocity among the  $P$  rotors.

According to (25) and (26), the Doppler spectrum of UAVs is spread over a frequency band with thin spectral lines equally spaced at a certain chopping frequency. If the MD signature is obtained from rotating blades with different angular velocities as shown in Fig. 2(a), the Doppler spectrum of the rotating blades becomes Fig. 2(b); for  $\omega_1 > \omega_2$ , the spectral line interval caused by  $\omega_1$  is longer than that caused by  $\omega_2$ . In general, the rotors of an actual flying multirotor UAV have quite similar angular velocities. If four

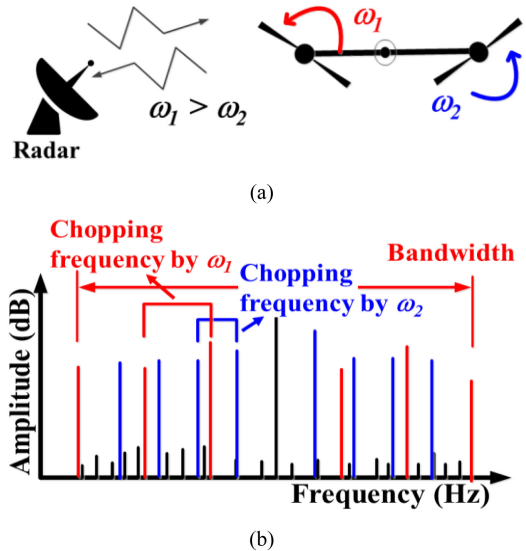


Fig. 2. MD signature in the frequency domain against rotating blades with different angular velocities. (a) Measurement geometry. (b) Doppler spectrum.

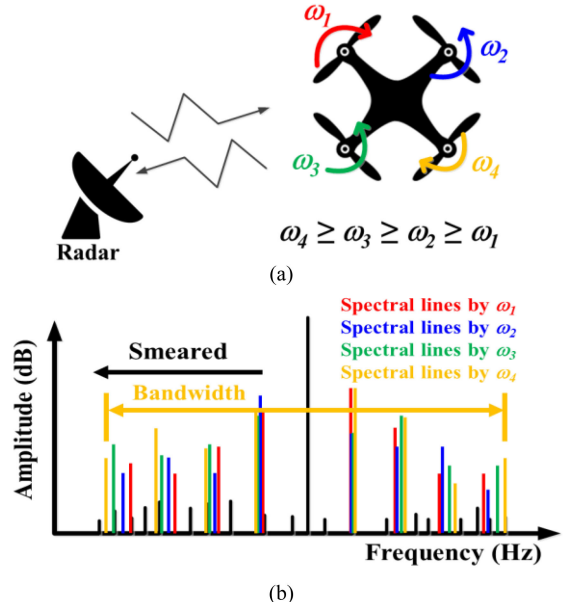


Fig. 3. MD signature in the frequency domain against the multirotor UAV with four rotors. (a) Measurement geometry. (b) Doppler spectrum.

rotors with slightly different angular velocities are rotating as shown in Fig. 3(a), the Doppler spectrum obtained from the quadcopter of Fig. 3(a) becomes severely smeared at relatively high frequencies [see Fig. 3(b)]; the spectral lines are spaced at the integer multiples of each chopping frequency.

### C. Analysis of Doppler Spectrum Using Point Scatter Model

To demonstrate the relationships between the foregoing parameters related to the dynamics of small UAVs and the MD features (e.g., chopping frequency and Doppler bandwidth), simulations were performed using two categories of small UAV models: fixed-wing and rotary-wing models,

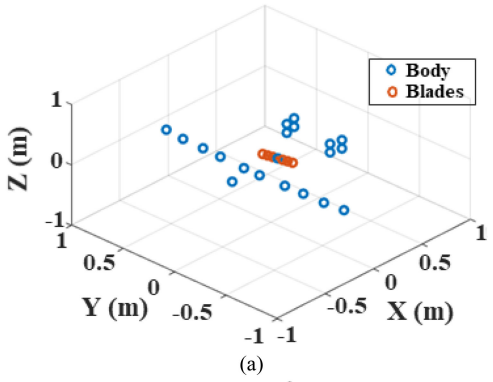


Fig. 4. Point scatterer models: (a) fixed-wing and (b) rotary-wing UAVs.

TABLE I  
Simulation Parameters for Doppler Spectrum Analysis

Center frequency	9.85 GHz
Pulse repetition frequency	35 kHz
CPI	0.0857 s
Number of bursts	3000
Number of blades on each rotor ( $N$ )	2

TABLE II  
Parameters Corresponding to Six Different Scenarios

Scenario	Small UAV model	Blade length ( $r$ )	RPM	Number of rotors ( $P$ )	Radial velocity ( $v$ )	Angle between TPP and LOS ( $\beta$ )
Type 1	Fixed wing	15 cm	3500	1	0 m/s	0°
Type 2	Fixed wing	30 cm	3500	1	0 m/s	0°
Type 3	Fixed wing	15 cm	7000	1	0 m/s	0°
Type 4	Rotary wing	15 cm	3395–3500	4	0 m/s	0°
Type 5	Rotary wing	15 cm	3395–3500	4	-20 m/s	0°
Type 6	Rotary wing	15 cm	3395–3500	4	0 m/s	60°

consisting of ideal point scatterers (see Fig. 4). In this simulation, the Doppler spectrum was analyzed against six different scenarios with five varying parameters: number of rotors ( $P$ ), angular velocity of rotor, blade length ( $r$ ), and angle between TPP and LOS ( $\beta$ ); the detailed simulation parameters are listed in Tables I and II. The six target

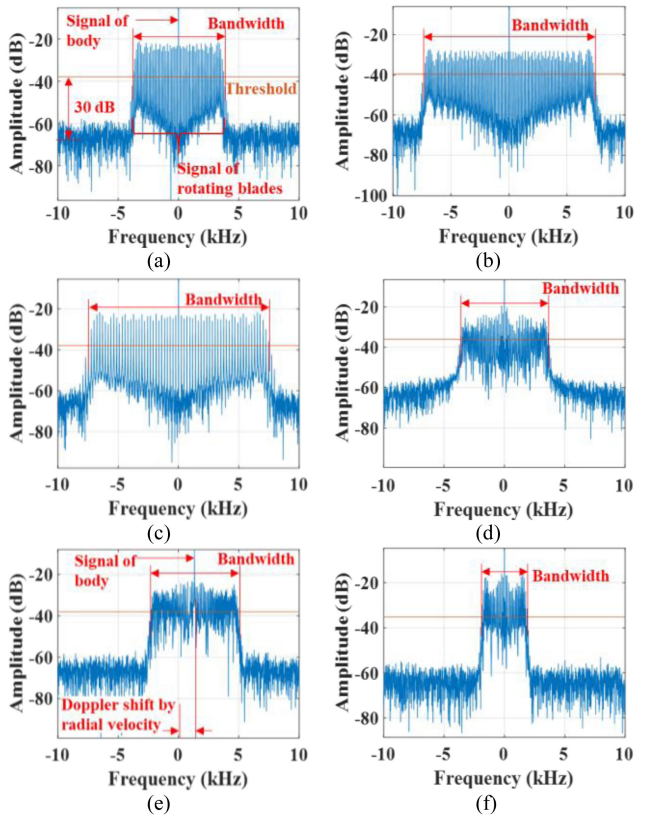


Fig. 5. Doppler spectrum corresponding to six different scenarios: (a) Type 1, (b) Type 2, (c) Type 3, (d) Type 4, (e) Type 5, and (f) Type 6.

types consisting of point scatterers (see Table II) are classified into fixed-wing (Types 1–3) and rotary-wing models (Types 4–6). The r/min and the length of a blade in Table II are selected considering physical specifications of the real small UAVs [39], [48], [49].

The Doppler spectrum of six different scenarios with different parameter settings is shown in Figs. 5 and 6; the Doppler spectrum in Fig. 6 is the magnified view of Fig. 5. As shown in Figs. 5 and 6, it is clear that the Doppler spectrum consists of spectral lines spaced at a certain frequency interval and spreads over a wide frequency band around the body signal. Table III lists the measured Doppler bandwidths and interval between spectral lines, i.e., chopping frequency and their theoretical values. As shown in Table III, the measured values are considerably similar to the theoretical values, which are calculated by substituting the parameters listed in Tables I and II into (25) and (26). The Doppler bandwidth was determined by the frequency range of a signal exceeding a threshold, which was 30 dB above the mean amplitude of the Doppler spectrum in the range  $\pm 8$  to  $\pm 10$  kHz. The chopping frequency was determined by the difference between the first and second spectral lines in the positive frequency band, except for the spectral line from the main body.

The only difference between Types 1 and 2 is the blade length, i.e., that of Type 2 is twice that of Type 1. According to (26), when the blade length is doubled, the Doppler bandwidth also doubles, which can be easily verified by comparing Fig. 5(a) and (b). If we investigate the Doppler

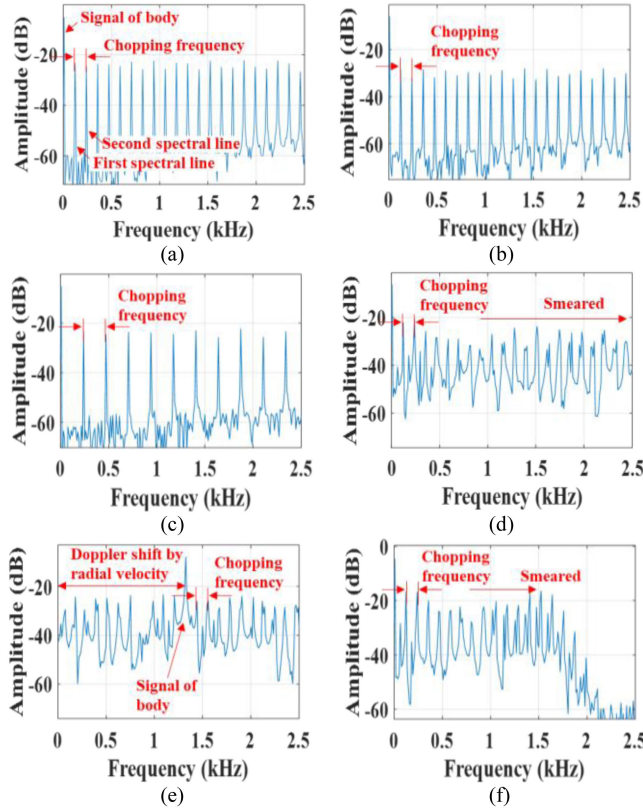


Fig. 6. Doppler spectrum in frequency range 0–2500 Hz corresponding to six different scenarios: (a) Type 1, (b) Type 2, (c) Type 3, (d) Type 4, (e) Type 5, and (f) Type 6.

TABLE III  
MD Features Obtained From Doppler Spectrum at Six Different Scenarios

Scenario	Feature	Theoretical value	Measured value
Type 1	Bandwidth	7220.4 Hz	7469.2 Hz
	Chopping frequency	116.67 Hz	116.70 Hz
Type 2	Bandwidth	14 441 Hz	14 705 Hz
	Chopping frequency	116.7 Hz	116.7 Hz
Type 3	Bandwidth	14 441 Hz	14 938.0 Hz
	Chopping frequency	233.33 Hz	233.50 Hz
Type 4	Bandwidth	7220.4 Hz	7235.7 Hz
	Chopping frequency	116.67 Hz	116.70 Hz
Type 5	Bandwidth	7220.4 Hz	7235.7 Hz
	Chopping frequency	116.67 Hz	117.00 Hz
	Doppler shift by radial velocity	1313.3 Hz	1325.0 Hz
Type 6	Bandwidth	3610.2 Hz	3617.9 Hz
	Chopping frequency	116.67 Hz	116.70 Hz

bandwidth of a small UAV, then we can obtain the information on the lengths of rotating blades.

The angular velocity of Type 3 blades is two times faster than that of Type 1 blades. According to (25) and (26), the blade rotation modulates the chopping frequency

as well as Doppler bandwidth, which are directly proportional to the angular velocity of the blade, respectively. These phenomena are clearly shown in Fig. 5(a) and (c) for Doppler bandwidth, and Fig. 6(a) and (c) for chopping frequency, respectively. Provided that the Doppler bandwidth and chopping frequency can be measured, information can be obtained on the angular velocity of a rotating blade; this information is considerably useful for the detection and classification of small UAVs.

The simulation of Type 4 was performed using the rotary-wing UAV model with four rotors [see Fig. 4(b)]. When the rotary-wing UAV moves in a specific direction, the angular velocities of the different rotors usually differ; accordingly, this situation is reflected by varying the angular velocity of the four rotors from 3395 to 3500 r/min. In Type 4, the other parameters (except for the angular velocity and number of rotors) are the same as those of Type 1. The blade length is the same as that of Type 1, and the maximum rotation of Type 4 is 3500 r/min, similar to that of Type 1. The MD features of Type 4 are similar to those of Type 1, as listed in Table III. In Type 4, the four rotors with slightly different angular velocities induce four different chopping frequencies. The spectral lines are spaced at the integer multiples of each chopping frequency; hence, the Doppler spectrum of Type 4 becomes severely smeared at relatively high frequencies [see Fig. 6(d)]. As a result, the distribution of the Doppler spectrum between Types 1 and 4 exhibits a distinct difference [see Fig. 6(a) and (d)] although the angular velocities of the rotors are quite similar.

In the investigation of the MD effect in the frequency domain, it is found that the MD features obtained from the Doppler spectrum and its distribution provide considerably useful information on the parameters related to the dynamics of small UAVs (e.g., blade length, angular velocity, and number of rotors). These characteristics can possibly be utilized to detect small UAVs with a low RCS or to discriminate between small UAVs and other objects, such as birds and clutter with a high RCS and without rotating blades. However, the Doppler spectrum of a small flying UAV can be modulated by other parameters in addition to those previously mentioned.

The parameters of Type 5 (see Table II) are nearly the same as those of Type 4; however, the former has a radial velocity of  $-20$  m/s instead of  $0$  m/s. According to (26), the radial velocity of a small UAV shifts the center of the Doppler spectrum from  $0$  Hz to approximately  $1313.3$  Hz [see Figs. 5(e) and 6(e) and Table III]. In Type 6, the angle between the TPP and LOS ( $\beta$ ) is  $60^\circ$ , and the other parameters are the same as those of Type 4. Owing to the scaling factor,  $\cos(\beta)$ , in (26),  $\beta$  reduces the bandwidth of the Doppler spectrum. These facts are consistent with the phenomena shown in Figs. 5(f) and 6(f); the detailed values are listed in Table III. It should be noted that the Doppler bandwidth and chopping frequency might not provide the exact physical specifications of a small UAV in a situation where the radial velocity and  $\beta$  are unknown and unpredictable.

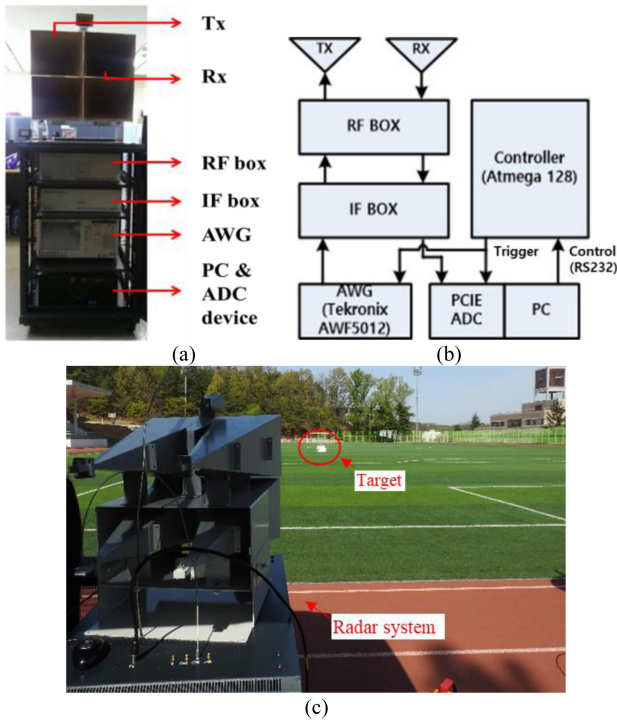


Fig. 7. Measurement setup: (a) X-band radar, (b) block diagram, and (c) measurement environment.

TABLE IV  
Experimental Parameters of X-Band Radar System

Center frequency	9.85 GHz
Bandwidth	20 MHz
Pulse repetition frequency	20–30 kHz
Coherent integration time (CPI)	0.08 s
Transmission power	29.8 dBm (maximum)
Antenna beam width	20°
Polarization	HH

### III. MEASUREMENT RESULTS

In this section, the measured data of various types of small UAVs were used to investigate their MD signatures. The X-band radar measurement system [see Fig. 7(a)] transmits a linear frequency modulation waveform and receives an echo signal reflected from a small UAV. An arbitrary waveform generator (AWG) generates the modulated waveform, and the intermediate and radio frequency boxes shift the center frequency to the X-band [see Fig. 7(b)]. To obtain the MD signatures, the signal phase coherence is considerably important. For this purpose, the ATmega128 microprocessor generates the trigger signal to synchronize the AWG and analogue to a digital converter, and the host computer with the RS-232 controls the microprocessor. The measurement setup and parameter details of the X-band radar system are shown in Fig. 7 and summarized in Table IV, respectively.

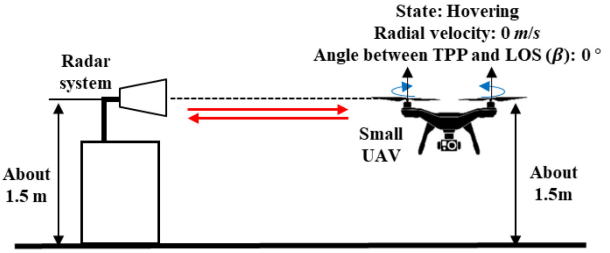


Fig. 8. Measurement geometry for small UAVs without radial velocity at  $\beta = 0^\circ$ .

TABLE V  
Physical Parameters of Four Small UAV Models

	Fixed-wing UAV	Quadcopter	Hexacopter	RC helicopter
Number of rotors	1	4	6	2
Blade length	15 cm	12 cm	30 cm	40.7 cm
Number of blades on each rotor	2	2	2	2

#### A. MD Signature Analysis Without Radial Velocity at $\beta = 0^\circ$

To demonstrate the relationship between the MD features and dynamics of small UAVs when the radial velocity is 0 m/s and the angle ( $\beta$ ) between TPP and LOS is  $0^\circ$  (see Fig. 8), the MD signatures are measured against four small UAV models: 1) fixed-wing UAV [48]; 2) quadcopter [49]; 3) hexacopter; and 4) remote control (RC) helicopter [50] (see Fig. 9 and Table V). As demonstrated in the previous section, the measured MD signatures of the four small UAVs are spread over a wide frequency band around the body signal on the Doppler spectrum (see Figs. 10 and 11). These MD signatures consist of spectral lineequally spaced at a chopping frequency on the Doppler spectrum.

The measured MD features (i.e., Doppler bandwidth and chopping frequency) are summarized in Table VI. In the measurement results, the power level of the MD components is quite low compared to that of the body signal (see Table VII). However, the body signal can be easily eliminated by using a band-rejection filter, because the body signal is concentrated in very narrow frequencies. Then, the MD signature can be clearly observed on both the Doppler spectrum and the JTF images. After eliminating the body signal, the MD features were measured in the same way as in the previous session except that the 20 dB was used instead of 30 dB. The Doppler bandwidths against four small UAV models significantly differ in the range 5000–15 000 Hz. Each small UAV model also has a different chopping frequency and rotation period.

Provided that the exact number of rotor blades is known, the angular velocity and blade length can be estimated by substituting the measured MD features into (25) and (26). In general, the angular velocity of a small UAV is in the range 150.8–628.3 rad/s [30], [36], [39], and the estimated angular velocities against four small UAVs are all within this range (see Table VI). In addition, the estimated blade length for



Fig. 9. Optical image of four small UAV models: (a) fixed-wing UAV, (b) quadcopter, (c) hexacopter, and (d) RC helicopter.

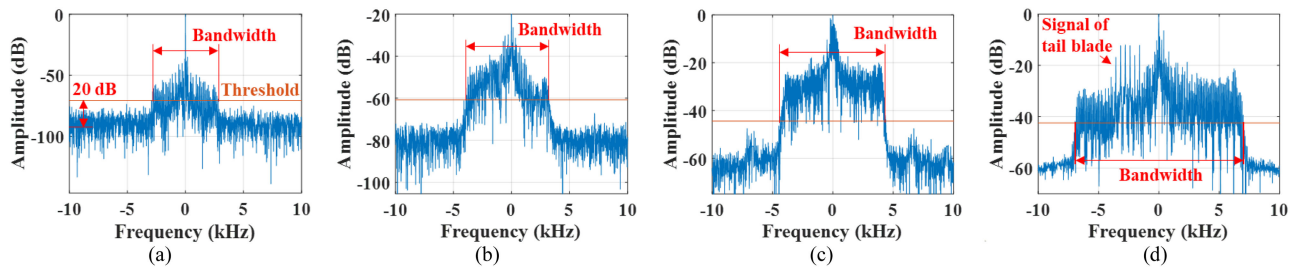


Fig. 10. Doppler spectrum against four small UAVs: (a) fixed-wing UAV, (b) quadcopter, (c) hexacopter, and (d) RC helicopter.

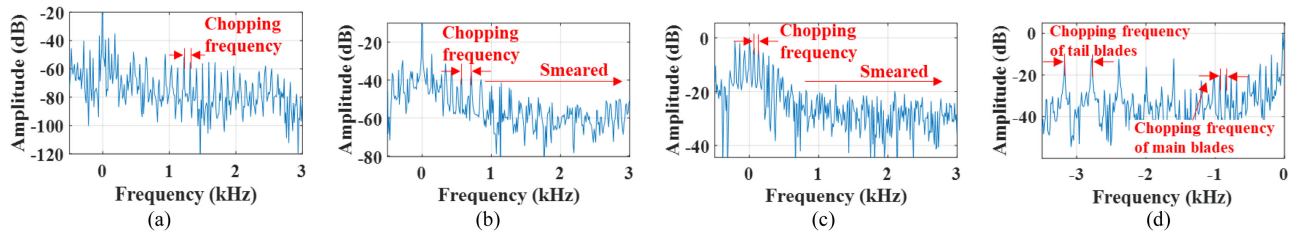


Fig. 11. Magnified view of Doppler spectrum for four small UAVs: (a) fixed-wing UAV, (b) quadcopter, (c) hexacopter, and (d) RC helicopter.

TABLE VI  
Measured MD Features and Estimated Parameters of Small UAVS Against Four Small UAVs

	Fixed-wing UAV		Quadcopter		Hexacopter		RC Helicopter	
	Doppler spectrum	JTF image						
Measured Doppler bandwidth	5647.6 Hz	5522.5 Hz	7093.3 Hz	7502.4 Hz	8761.7 Hz	8767.1 Hz	13 918.0 Hz	14 167.0 Hz
Measured chopping frequency	94.00 Hz	.	140.00 Hz	.	70.00 Hz	.	82.00 Hz	.
Measured rotation period	.	0.02130 s	.	0.01400 s	.	0.02900 s	.	0.02410 s
Estimated angular velocity	295.31 rad/s	294.99 rad/s	439.82 rad/s	448.80 rad/s	219.91 rad/s	216.66 rad/s	257.61 rad/s	260.71 rad/s
Estimated length of a blade	16.03 cm	15.69 cm	13.51 cm	14.01 cm	33.39 cm	33.91 cm	45.27 cm	45.54 cm

TABLE VII  
Amplitude Difference Between MD Signature and Body Signal

	Fixed-wing UAV	Quadcopter	Hexacopter	RC helicopter
Doppler spectrum	-39 ~ -23 dB	-45 ~ -26 dB	-25 ~ -10 dB	-10 ~ 24 dB
JTF image	-26 ~ -20 dB	-34 ~ 25 dB	-22 ~ -14 dB	-15 ~ -12 dB

each small UAV (see Table VI) is considerably similar to the actual blade lengths listed in Table V. In other words, it was confirmed that the relationship between the dynamics

of small UAVs and the MD features of small UAVs can be completely explained by utilizing (25) and (26).

Many researchers have already shown that the JTF image can provide useful features related to the motion dynamics of small UAVs [35], [36]. In order to show the usefulness of the Doppler spectrum, we compared the MD features and parameters obtained from the Doppler spectrum with those obtained from the JTF images. The MD signatures of the measured data in the JTF domain are shown in Fig. 12. They show periodical flashes covering a specific range of frequencies. As shown in [35], the Doppler bandwidth determined by the flashes and the flash period formed by a single blade are crucial features in the JTF image.

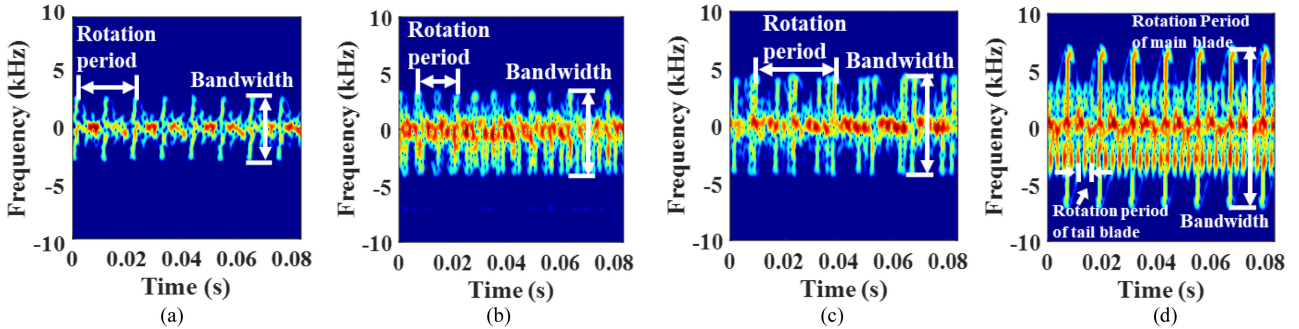


Fig. 12. JTF images against for small UAVs: (a) fixed-wing UAV, (b) quadcopter, (c) hexacopter, and (d) RC helicopter.

The Doppler bandwidth measured from the JTF images can provide useful information related to the blade length and the angular velocity, but it can also be obtained by using the Doppler spectrum, instead of the JTF image (see Table VI). The flash period in the JTF image offers the information related to the angular velocity of the rotor, but such information can also be acquired using the chopping frequency on the Doppler spectrum. In addition, the results show that the estimated values of angular velocity and blade length based on the Doppler spectrum are similar to those based on the JTF images. In other words, the Doppler spectrum can provide as accurate values of the MD features as the JTF images. It is noteworthy that the Doppler spectrum is a useful tool to investigate the MD signatures of small UAVs, compared to the JTF image.

Moreover, we found that the Doppler spectrum of rotary-wing UAVs [see Fig. 11 (b) and (c)] are considerably smeared at relatively high frequencies even when they are hovering without radial motion. Although the rotary-wing UAV remains in the same position in air, it occasionally tilts because of turbulence, gyroscope inaccuracy, and component imbalance. To stabilize the hover of rotary-wing UAVs, the thrust in each of the rotors should be continuously adjusted for their angular velocities to vary during the measurement. Rotating blades with slightly different angular velocities induce spectral lines with different chopping frequencies; hence, the Doppler spectrum obtained from rotary-wing UAVs are smeared in the frequency domain, even as the UAVs hover [see Fig. 11(b) and (c)]. In contrast, the Doppler spectrum of the fixed-wing UAV in Fig. 9(a) seems to exhibit clear chopping frequencies without smearing [see Fig. 11(a)]. A fixed-wing UAV usually has one or two rotors; hence, it is common for the angular velocities of these rotors to remain constant during brief measurement periods. If *a priori* information on the number of rotors is available, then it is possible to discriminate between fixed-wing and rotary-wing UAVs; the rotary wing UAVs usually have more than four rotors, and fixed wing UAVs usually have up to two rotors. Thus, if the degree of smearing on the Doppler spectrum can be measured, then the fixed-wing and rotary-wing UAVs may be discriminated.

Additionally, it is noteworthy that the distribution of the Doppler spectrum and JTF image of the RC helicopter [see Figs. 10(d), 11(d), and 12(d)] completely differ from

TABLE VIII  
Measured MD Features of Tail Blades and Analysis Results Related to Tail Blades of RC Helicopter

	Doppler spectrum	JTF image
Measured chopping frequency	397.00 Hz	.
Measured rotation period	.	0.0051 s
Estimated angular velocity	1247.21 rad/s	1232.00 rad/s
Tail gear ratio		4.73:1
Estimated ratio	4.84:1	4.73:1

TABLE IX  
Measured MD Features and Estimated Parameters of Small UAVs Against Two Maneuvering Small UAVs

	Fixed-wing UAV		Quadcopter	
	Doppler spectrum	JTF image	Doppler spectrum	JTF image
Doppler frequency shifted by radial velocity	921.7 Hz	922.9 Hz	653.4 Hz	625.0 Hz
Estimated radial velocity	15.45 m/s	15.47 m/s	10.95 m/s	10.47 m/s
Measured Doppler bandwidth	6160.0 Hz	6511.2 Hz	8284.7 Hz	7851.6 Hz
Measured chopping frequency	157.5 Hz	.	163.3 Hz	.
Measured rotation period	.	0.0130 s	.	0.0129 s
Estimated angular velocity	494.8 rad/s	483.3 rad/s	513.02 rad/s	487.07 rad/s
Estimated blade length	.	.	13.53 cm	13.51 cm

those of other small UAVs. The spectra lines induced by the main and tail blades are identified together in the frequency domain. In the JTF domain, several flashes caused by the tail blades are formed between the flashes caused by the main blades. The angular velocity of the tail rotor (see Table VIII) is considerably faster than that of the main rotor (see Tables VI). The estimated ratio in Table VIII represents the ratio between the measured angular velocities of the main and tail blades; it is very similar to the specified gear ratio of the RC helicopter model [50]. This characteristic is extremely unique compared with those of other small UAVs; hence, it



Fig. 13. Fixed-wing UAV model: number of rotors is two, blade length is 20 cm, and number of blades is two.

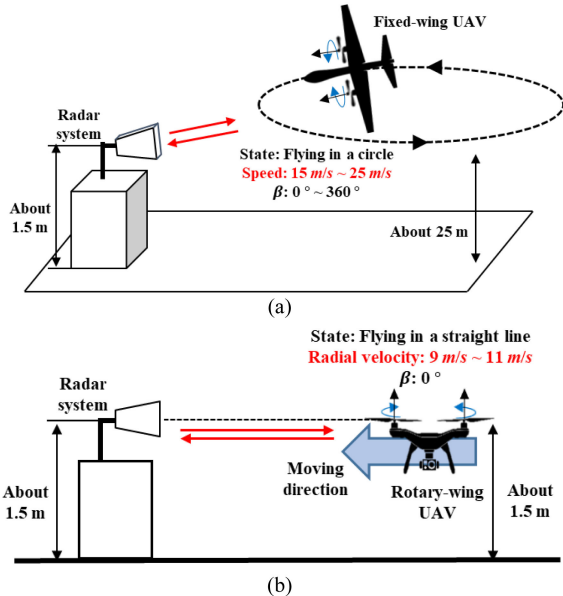


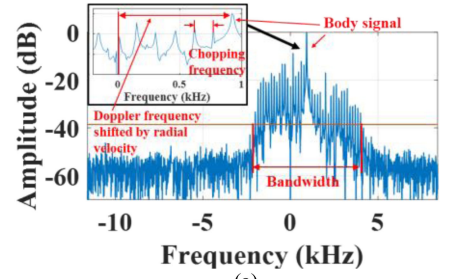
Fig. 14. Measurement geometry for (a) fixed-wing UAV flying in a circle and (b) rotary-wing UAV flying in a straight line.

can be used to detect and differentiate the RC helicopters from other types of small UAVs.

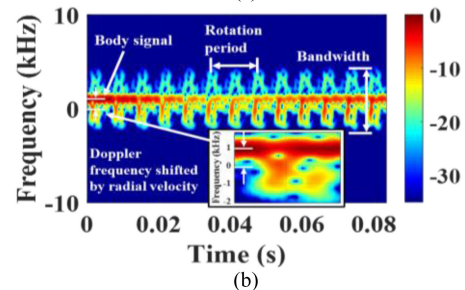
Based on the above investigations, the observation of MD signatures using the measured data from the Doppler spectrum can provide a considerable amount of useful information for the detection and classification of small UAVs. However, in practical situations, certain factors, such as the translational motion and the angle ( $\beta$ ) between the TPP and LOS, can further modulate the signal of a small UAV with rotating blades. As presented in Section III, this modulation makes it difficult to predict the dynamics of small UAVs from its MD features. Accordingly, further analyses considering the translational motion and  $\beta$  are discussed in the next section.

### B. MD Signature Analysis With Translational Motion

To analyze the effects of translational motion using the MD signatures of small UAVs, experiments were performed on the fixed-wing UAV (see Fig. 13) and quadcopter [see Fig. 9(b)] flying around a circle and along a straight line (see Fig. 14), respectively. The Doppler spectrum and JTF images of two small UAVs are shown in Figs. 15 and 16. The Doppler spectrum of two small UAVs is spread over a frequency bandwidth with thin spectral lines equally spaced at a certain chopping frequency. In addition, the distribution of both the Doppler spectrum and JTF images are shifted in

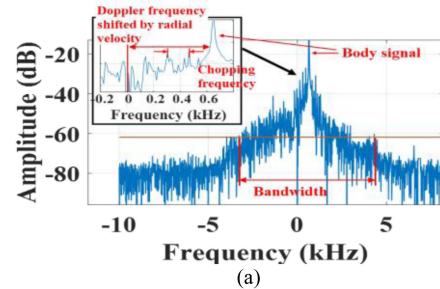


(a)

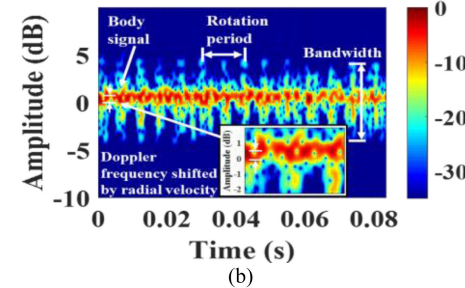


(b)

Fig. 15. MD signatures against fixed-wing UAV flying in a circle [see Fig. 14]: (a) Doppler spectrum and (b) JTF image.



(a)



(b)

Fig. 16. MD signatures against quadcopter flying in a straight line [see Fig. 14(b)]: (a) Doppler spectrum and (b) JTF image.

the frequency domain due to the translational motion of the maneuvering small UAVs.

During the measurement of the MD signatures of the two small UAVs, the speeds of the fixed-wing and rotary-wing UAVs changed from 15 to 25 m/s and from 9 to 11 m/s, respectively. In other words, the translational motion of the two small UAVs included both the velocity and acceleration during the measurement time. In the JTF image, we can observe instantaneous frequency caused by the change of the speed. However, the Doppler spectrum can be severely smeared by the acceleration. If the change in the speed of a small UAV was not negligible during the measurement time, it would be more appropriate to investigate the MD signature using the JTF image rather than the Doppler spectrum. However, the additional modulation induced by the acceleration

TABLE X  
Measured MD Features and Estimated Parameters of Small UAVs Against Two Small UAVs with  $\beta$  Variations

Type of small UAV	$\beta$	Method	Measured Doppler bandwidth	Measured chopping frequency	Measured rotation period	Estimated angular velocity	Estimated blade length (Assuming $\beta = 0^\circ$ )
Fixed-wing UAV	30°	Doppler spectrum	4924.2 Hz	93.3 Hz	.	293.11 rad/s	14.08 cm
		JTF image	4848.6 Hz	.	0.02147 s	292.65 rad/s	13.88 cm
	60°	Doppler spectrum	2753.8 Hz	93.4 Hz	.	293.42 rad/s	7.86 cm
		JTF image	2739.3 Hz	.	0.02174 s	289.01 rad/s	7.94 cm
Quadcopter	90°	Doppler spectrum	1190.2 Hz	81.7 Hz	.	256.64 rad/s	3.89 cm
		JTF image	1157.2 Hz	.	.	.	.
	23°	Doppler spectrum	7187.9 Hz	163.4 Hz	.	513.34 rad/s	11.73 cm
		JTF image	7031.3 Hz	.	0.01214 s	517.56 rad/s	11.38 cm
	40°	Doppler spectrum	5554.3 Hz	175.0 Hz	.	549.78 rad/s	8.47 cm
		JTF image	5576.2 Hz	.	0.01150 s	546.36 rad/s	8.55 cm

was not identified on both the Doppler spectrum and the JTF images (see Figs. 15 and 16), due to the small amount of acceleration as well as short measurement time, which is the case for most of operational radars.

As shown in simulation in the previous section, the radial velocity causes the Doppler shift in the frequency domain. By using the Doppler-shifted frequencies of the body signal, the radial velocities against the two small UAVs were estimated (see Table IX). All of the estimated radial velocities are within the range of the actual speed of each small UAV. In addition, the MD features measured from the maneuvering quadcopter (see Table IX) do not considerably differ from those of the quadcopter hovering at the same position (see Table VI); the estimated blade length from the maneuvering quadcopter is similar to the actual blade length (see Table V).

When a small UAV is moving in a specific direction, its translational motion additionally modulates the MD signature of its rotating blades. However, due to the small acceleration and the short measurement time, the spectral distribution of maneuvering small UAVs were only shifted in the frequency domain without smearing of thin spectral lines. Therefore, it is likely that for most of operational radars having very short CPI, the MD signatures of small flying UAVs can be easily observed by using the Doppler spectrum, even if these UAVs maneuver toward any direction.

### C. MD Signature Analysis Against $\beta$

To observe the change in the MD features of small UAVs with respect to the variation of  $\beta$ , the MD signatures of the fixed-wing UAV [see Fig. 9(a)] and quadcopter [see Fig. 9(b)] were measured against various values of  $\beta$ . The variations in  $\beta$  for fixed-wing and rotary-wing UAVs are mainly caused by their movement directions and altitudes, respectively. Thus, to measure the MD signatures of small UAVs at various  $\beta$  values, the azimuth angles and altitudes

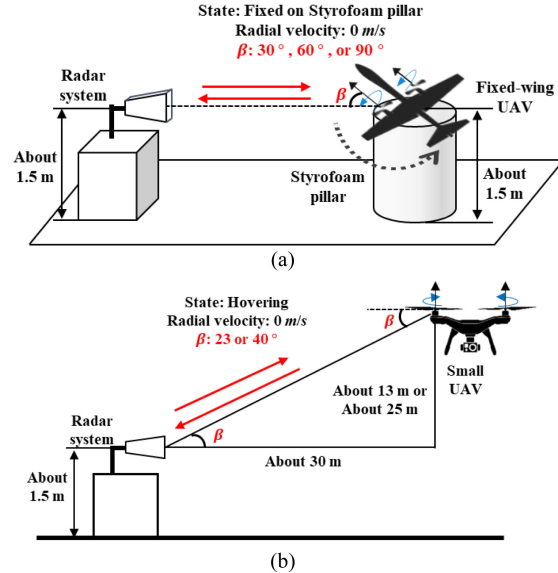


Fig. 17. Measurement geometry for (a) fixed-wing UAV and (b) quadcopter with variations of  $\beta$ .

of the fixed-wing UAV [see Fig. 17(a)] and quadcopter [see Fig. 17(b)] were altered, respectively.

Although the MD signatures are obtained at different values of  $\beta$  (see Figs. 18 and 19), the chopping frequency measured from the same small UAV does not exhibit any significant variation; the measured rotation period also has an extremely small variation (see Table X). However, on both the Doppler spectrum and the JTF images, the measured Doppler bandwidth drastically decreases as  $\beta$  increases because of the scaling factor ( $\cos\beta$ ) in (26). On the other hand, the Doppler bandwidth measured from the real fixed-wing UAV at  $\beta = 90^\circ$  did not converge to exactly zero due to the residual MD signatures and body signal.

By using the measured MD features, the angular velocity and blade length were estimated when  $\beta$  was unknown (i.e., under the assumption  $\beta = 0^\circ$ ) (see Table X). The estimated angular velocities of the small UAVs are considerably

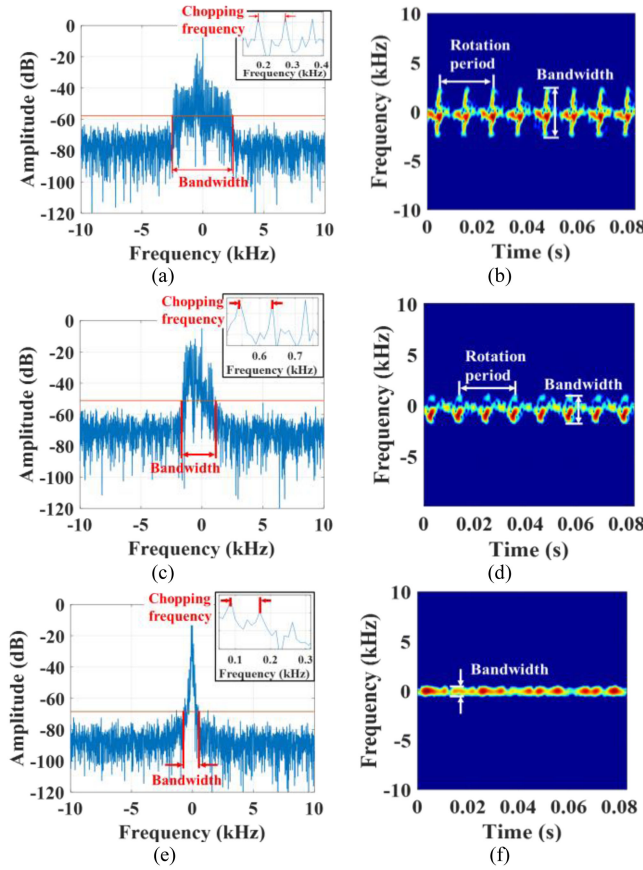


Fig. 18. (a), (c), and (e) Doppler spectrum and (b), (d), and (f) JTF images against fixed-wing UAV at (a) and (b)  $\beta = 30^\circ$ , (c) and (d)  $\beta = 60^\circ$ , and (e) and (f)  $\beta = 90^\circ$ .

similar; however, the estimated blade length decreases as  $\beta$  increases. Accordingly, the estimated blade length against a relatively high  $\beta$  significantly differs from the actual blade length in Table V.

A radar system without a tracking function can provide information regarding the object's location but not its exact movement directions and altitudes. This radar system can encounter difficulty in estimating the blade length because of an unknown  $\beta$  in (26). However, even without the information on  $\beta$ , the angular velocity of rotors can be estimated using the chopping frequency. Moreover, if the tracking radar, which can provide the information on  $\beta$  by using the movement directions and altitudes of the object, is available, then the exact blade length can be predicted by using the Doppler spectrum. Thus, even with significant variations in  $\beta$ , it is apparent that the foregoing information on the angular velocity and blade length facilitates the detection and classification of small UAVs.

#### D. Comparative Analysis of Doppler Spectrum and JTF Image

In the above-mentioned experimental analysis, the changes in the MD signatures relative to the physical specifications of small UAVs (e.g., blade length and rotor rotation rate) were successfully explained and predicted based on the Doppler spectrum. It was also verified that not only

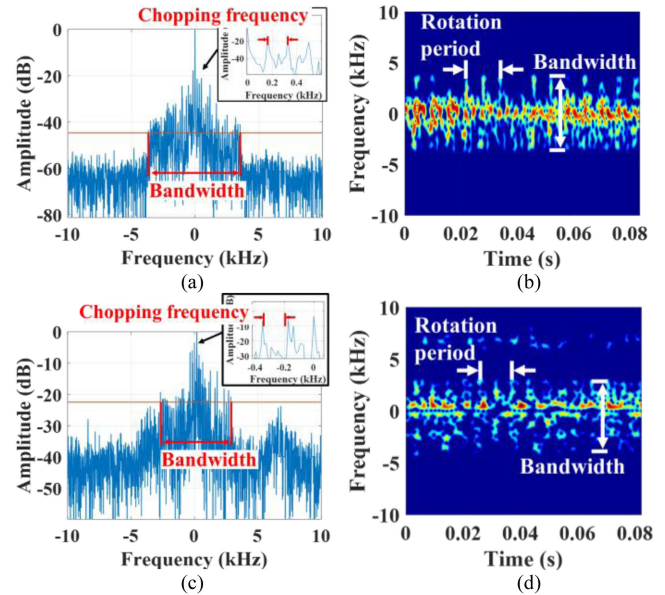


Fig. 19. (a) and (c) Doppler spectrum and (b) and (d) JTF images against the quadcopter at (a) and (b)  $\beta = 23^\circ$ ; (c) and (d)  $\beta = 40^\circ$ .

the features obtained from the JTF images but also those obtained from the Doppler spectrum can provide useful information for detection and classification of the small UAVs.

In addition, the Doppler spectrum can be computed by taking merely a single FT, whereas the JTF image requires a large number of FTs. To compute a single fast FT (FFT) using radix-2 algorithm, it takes  $O(N \log_2 N)$  complexity where  $N$  is the length of measured data and  $O$  is the Big  $O$  notation, which describes the complexity of the function. The computational complexity of short time FT (STFT) (i.e., the JTF image) is  $O(MN_f \log_2 N_f)$  where  $M$  is the number of windowed segments and  $N_f$  is the number of the desired frequency bins [53], [54].  $M$  is usually a large number because time resolution must be high enough to separate the flashes due to the MD signature in the time domain; the windowed segments should be very narrow and overlapped. If the number of samples within each windowed segment is quite small, zero padding should be additionally performed in the frequency domain to increase the number of frequency bins for accurate observation of the Doppler bandwidth of rotating blades. Thus, the number of the frequency bins  $N_f$  as well as  $M$  must be sufficiently large such that both the time interval between consecutive flashes and Doppler bandwidth can be clearly observable in the JTF image. Therefore, the computational complexity to obtain a single JTF image is much larger than that of the Doppler spectrum, which requires only a single  $N$ -point FFT.

In order to compare the computation times of the FFT and STFT, we performed 1000 Monte Carlo simulations by using the MATLAB R2020b running under Windows 10 on an Intel i7 processor; the results are shown in Fig. 20. For  $N = 2000$ , the FFT was 19 to 46 times faster than STFT, and for  $N = 10000$ , FFT was 22 to 77 times faster than STFT. These results show that the Doppler spectrum is highly computationally efficient, compared to the JTF

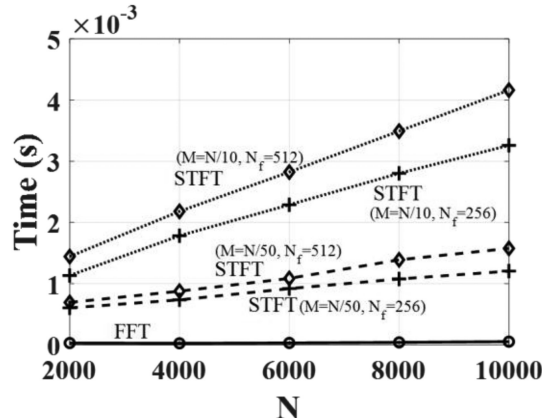


Fig. 20. Comparison of computational time of FFT and STFT.

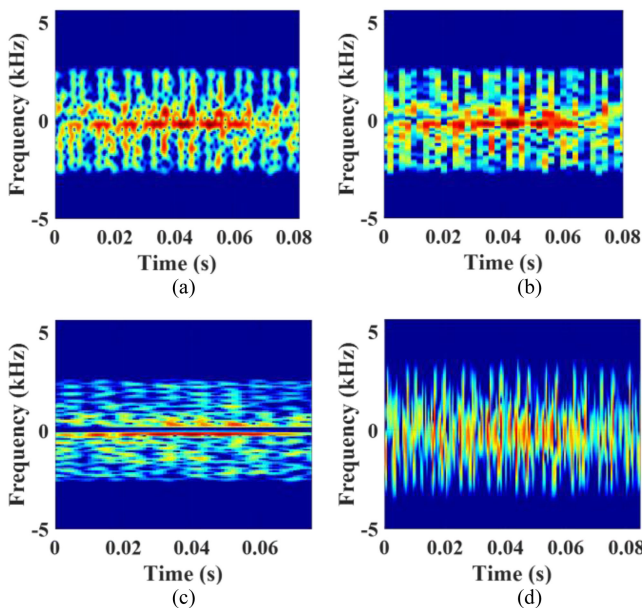


Fig. 21. JTF images against the quadcopter: (a)  $N_t = 80$  (4 ms) and  $\rho = 72$  (90% overlap), (b)  $N_t = 80$  (4 ms) and  $\rho = 40$  (50% overlap), (c)  $N_t = 200$  (10 ms) and  $\rho = 180$  (90% overlap), and (d)  $N_t = 20$  (1 ms) and  $\rho = 18$  (90% overlap).

image. In addition, a single JTF image requires a storage space of  $M \times N_f$ . This implies that classification of small UAVs requires a huge amount of the storage space, because it is necessary to collect a very large number of JTF images against various UAVs and flying scenarios.

In Fig. 21, it is clearly demonstrated that the quality of the JTF images is heavily dependent on the user parameters [32], [33], i.e., the size of windowed segments  $N_t$  and the number of the overlapped samples  $\rho$  between consecutive windowed segments. Fig. 21 shows the JTF images of the quadcopter [see Fig. 9(b)] by varying  $N_t$  and  $\rho$ . As shown in Fig. 21(a) and (b), when the adjacent windowed segments overlap less than 50%, the quality of the JTF image is significantly degraded. In Fig. 21(c), the JTF image with long  $N_t$  fails to provide sufficient information on the rotation period of the blades (i.e., time interval between flashes), because of the increased size of the windowed segment in STFT. If  $N_t$  is too shortened, the JTF image [see Fig. 21(d)] rather becomes severely blurred in the frequency domain,



Fig. 22. Photograph of measured bird.

due to the poor frequency resolution. Thus, when using the JTF image for extraction of the MD signatures of small UAVs, an appropriate choice of parameters for STFT is very essential to clearly observe both the flashes and the Doppler bandwidth of small UAVs. Unlike JTF images, the Doppler spectrum can be easily obtained without any selection of dedicated parameters.

#### E. MD Signature of Bird

Birds have an extremely low RCS, i.e., approximately  $-20$  dBsm [51], which is quite similar to that of small UAVs. If the transmission power of a radar is sufficiently high to detect small UAVs, then the radar system may also detect birds besides small UAVs. Birds generally fly by flapping their wings, producing a periodic and time-varying Doppler frequency shift. The similarity in terms of the RCSs and MD signatures prevents the discrimination between birds and small UAVs.

To observe the MD signature of a bird, the echo signals from a flying bird (see Fig. 22) were measured using the radar system shown in Fig. 7. Most birds flap their wings below 18 beats per second [52], generating MD signatures with considerably lower frequencies than small UAVs. Accordingly, the measurement was conducted for a considerably longer CPI (2.5 s) than that for small UAVs (0.02 s). This increase in CPI for a bird yielded a significantly improved Doppler resolution compared to that of small UAVs.

In the Doppler spectrum shown in Fig. 23(a), the bandwidth and chopping frequency generated by the flapping of wing cannot be distinctly identified because of the smear effect caused by the acceleration of the bird during the measurement; the bird decelerated and accelerated during the measurement. In the JTF image shown in Fig. 23(b), the spectrum caused by the body of the flying bird varies with time from  $-340$  Hz to approximately  $316$  Hz. The flashes induced by the flapping wings were periodically modulated around the body signal, yielding a Doppler bandwidth of approximately  $300$  Hz and a flash period of approximately  $0.302$  s. It should be noted that the Doppler bandwidth and flash period of the bird are considerably narrower and longer than those of small UAVs, respectively. Therefore, a band-rejection filter with a notch filter with its center frequency of zero can remove most of the energy of birds in the frequency domain. In addition, most of the spectral lines of the small UAVs still remain at high frequencies, because the band-rejection filter has a sufficiently narrow stop bandwidth in order to reject signatures from birds only.

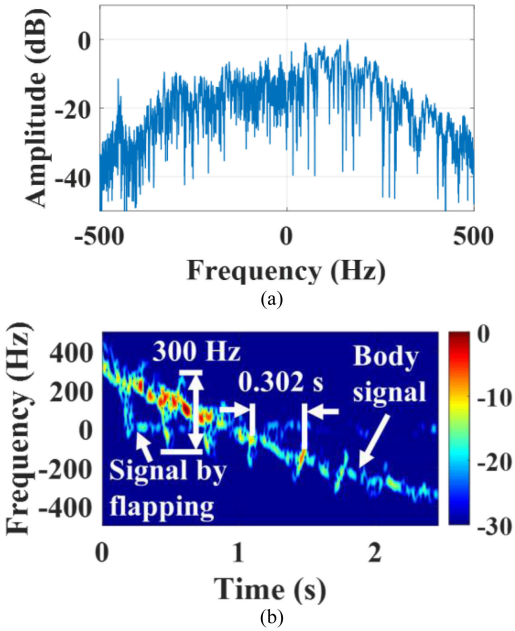


Fig. 23. MD signature of bird: (a) Doppler spectrum and (b) JTF image.

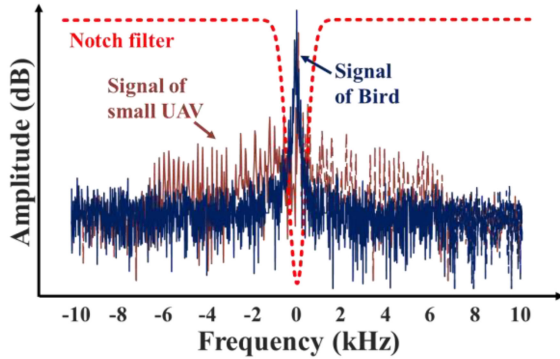


Fig. 24. Simple concept to reject bird energy in frequency domain; lines in dark red and dark blue represent Doppler spectrum against small UAV and bird, respectively; red line represents notch filter.

As a result, the small UAVs can be distinguished from birds, although echo signals of birds are measured with those of small UAVs (see Fig. 24).

#### IV. CONCLUSION

In this article, we established the concrete and theoretical foundation linking the MD signatures and motion dynamics of small UAVs, and analyzed the MD signatures of small UAVs based on the Doppler spectrum. For this investigation, we built a signal model in the time domain of a small flying UAV considering rotation rate of rotors, the length of a blade, the number of rotors, radial velocity, and aspect change. Subsequently, the corresponding spectral distribution in the frequency domain was theoretically derived and analyzed. Based on this, the actual physical specifications of a small UAV are compared with those obtained from the Doppler spectrum using simulations and measured data. In particular, experimental analysis was performed using the measurement data acquired from different types of small UAVs considering the radial velocity and aspect

change ( $\beta$ ). It is noteworthy that the analysis of the MD signatures based on the Doppler spectrum can provide richer amounts of information on the dynamics of small UAVs, compared with already existing studies, which mainly focus on only the phenomena observed in the measured data. In fact, we completely explained and predicted the changes in the Doppler spectrum against the motion dynamics of small UAVs. In addition, it was demonstrated that the Doppler spectrum, rather than the JTF image, is a considerably simple and useful tool for observing the MD signatures of small flying UAVs, in terms of both the computational time and the storage space.

It is assumed that the above analysis on the MD effects using the Doppler spectrum will significantly contribute to understanding the dynamics of small UAVs. Furthermore, the MD features introduced in this article may be used to detect and classify small UAVs. However, to utilize these MD features for the detection and classification of small UAVs, certain problems (e.g., the automatic estimation of chopping frequency, accuracy of estimated Doppler bandwidth, and smearing effects caused by multiple rotors on the Doppler spectrum) have to be resolved. In particular, it is a very difficult task to accurately extract the chopping frequency on the smeared Doppler spectrum; multiple peaks of the same magnitude will obviously prevent us from the detection of chopping frequencies. Therefore, in the future, we aim to formulate an algorithm for accurately and effectively detecting and classifying small UAVs with estimating the MD features.

#### REFERENCES

- [1] J. Vanian  
Drone registrations are still soaring  
*Fortune*, 2017. [Online]. Available: <http://fortune.com/2017/01/06/drones-registrations-soaring-faa>, Accessed on Nov. 14, 2017
- [2] J. S. Patel, F. Fioranelli, and D. Anderson  
Review of radar classification and RCS characterisation techniques for small UAVs or drones  
*IET Radar, Sonar Naviga.*, vol. 12, no. 9, pp. 911–919, Sep. 2018.
- [3] M. I. Skolnik  
*Introduction to Radar Systems*, 3rd ed. New York, NY, USA: McGraw-Hill, 2001.
- [4] B. R. Mahafza  
*Radar Systems Analysis and Design Using MATLAB*, 3rd ed. London, U.K.: Chapman and Hall/CRC, 2013.
- [5] M. Richards  
*Fundamentals of Radar Signal Processing*, 2nd ed. New York, NY, USA: McGraw-Hill, 2005.
- [6] J. Drozdowicz *et al.*  
35 GHz FMCW drone detection system  
In *17th Int. Radar Symp.*, 2016, pp. 1–4.
- [7] J. Klare, O. Bialawons, and D. Cerutti-Maori  
Detection of UAVs using the MIMO radar MIRA-CLE ka  
In *Proc. 11th Eur. Conf. Synthetic Aperture Radar*, 2016, pp. 1–4.
- [8] İ. Güvenç, O. Ozdemir, Y. Yapıcı, H. Mehrpouyan, and D. Matolak  
Detection, localization, and tracking of unauthorized UAS and jammers  
In *Proc. IEEE/AIAA 36th Digit. Avionics Syst. Conf.*, 2017, pp. 1–10.
- [9] M. Ezuma, O. Ozdemir, C. K. Anjinappa, W. A. Gulzar, and I. Guvenc  
Micro-UAV detection with a low-grazing angle millimeter wave radar  
in *Proc. IEEE Radio Wireless Symp.*, 2019, pp. 1–4.

- [10] C. M. Alabaster, E. J. Hughes, and D. W. Forman  
Is it a bird or is it a plane?"  
*In Proc. Int. Waveform Diversity Des. Conf.*, 2012, pp. 007–012.
- [11] S. Björklund  
Target detection and classification of small drones by boosting on radar micro-Doppler  
*In Proc. 15th Eur. Radar Conf.*, 2018, pp. 182–185.
- [12] A. Schroderet *et al.*  
Numerical and experimental radar cross section analysis of the quadrocopter DJI Phantom 2  
*In Proc. IEEE Radar Conf.*, 2015, pp. 463–468.
- [13] A. Herschfeldt *et al.*  
Consumer-grade drone radar cross-section and micro-Doppler phenomenology  
*In Proc. IEEE Radar Conf. Radar Conf.* 2017, pp. 0981–0985.
- [14] A. V. Khristenko *et al.*  
A system for measurement of electromagnetic wave scattered by small UAVs  
*In Proc. Int. Siberian Conf. Control Commun.*, 2017.
- [15] R. Guay, G. Drolet, and J. R. Bray  
Measurement and modelling of the dynamic radar cross-section of an unmanned aerial vehicle  
*IET Radar Sonar Navigat.*, vol. 11, no. 7, pp. 1155–1160, 2017.
- [16] B. Torvik, K. E. Olsen, and H. D. Griffiths  
X-band measurements of radar signatures of large sea birds  
*In Proc. Int. Radar Conf.*, 2014, pp. 1–6.
- [17] M. Ritchie, F. Fioranelli, H. Griffiths, and B. Torvik  
Monostatic and bistatic radar measurements of birds and micro-drone  
*In Proc. IEEE Radar Conf.*, 2016, pp. 1–5.
- [18] P. Molchanov, K. Egiazarian, J. Astola, R. I. A. Harmanny, and J. J. M. de Wit  
Classification of small UAVs and birds by micro-Doppler signatures  
*In Proc. Eur. Radar Conf.*, 2013, pp. 172–175.
- [19] V. C. Chen  
*The Micro-Doppler Effect in Radar*, 2nd ed. Norwood, MA, USA: Artech House, 2011.
- [20] V. C. Chen, F. Li, S. Ho, and H. Wechsler  
Micro-Doppler effect in radar: Phenomenon, model, and simulation study  
*IEEE Trans. Aerosp. Electron. Syst.*, vol. 42, no. 1, pp. 2–21, Jan. 2006.
- [21] S. Rahman and D. A. Robertson  
Classification of drones and birds using convolutional neural networks applied to radar micro-Doppler spectrogram images  
*IET Radar, Sonar Navigat.*, vol. 14, no. 5, pp. 653–661, 2020.
- [22] A. Huizing, M. Heiligers, B. Dekker, J. de Wit, L. Cifola, and R. Harmanny  
Deep learning for classification of Mini-uavs using micro-Doppler spectrograms in cognitive radar  
*IEEE Aerosp. Electron. Syst. Mag.*, vol. 34, no. 11, pp. 46–56, [40] Nov. 2019.
- [23] S. Björklund and N. Wadströmer  
Target detection and classification of small drones by deep learning on radar micro-Doppler  
*In Proc. Int. Radar Conf.*, 2019, pp. 1–6.
- [24] P. Zhang, G. Li, C. Huo, and H. Yin  
Exploitation of multipath micro-Doppler signatures for drone classification  
*IET Radar, Sonar Navigat.*, vol. 14, no. 4, pp. 586–592, 2020.
- [25] M. Ritchie, F. Fioranelli, H. Borrión, and H. Griffiths  
Multistatic micro-Doppler radar feature extraction for classification of unloaded/loaded micro-drones  
*IET Radar, Sonar Navigat.*, vol. 11, no. 1, pp. 116–124, 2017.
- [26] P. Zhang, L. Yang, G. Chen, and G. Li  
Classification of drones based on micro-Doppler signatures with dual-band radar sensors  
*In Proc. Prog. Electromagn. Res. Symp.–Fall*, 2017, pp. 638–643.
- [27] B. K. Kim, H. Kang, S. Lee, and S. Park  
Improved drone classification using polarimetric merged-Doppler images  
*IEEE Geosci. Remote Sens. Lett.*, to be published.
- [28] M. Ritchie, F. Fioranelli, H. Borrión, and H. Griffiths  
Multistatic micro-Doppler radar feature extraction for classification of unloaded/loaded micro-drones  
*IET Radar, Sonar Navigat.*, vol. 11, no. 1, pp. 116–124, 2017.
- [29] L. Fuhrmann, O. Bialawons, J. Klare, R. Panhuber, R. Klenke, and J. Ender  
Micro-Doppler analysis and classification of UAVs at ka band  
*In Proc. 18th Int. Radar Symp.*, 2017, pp. 1–9.
- [30] R. I. A. Harmanny, J. J. M. de Wit, and G. P. Cabic  
Radar micro-Doppler feature extraction using the spectrogram and the cepstrogram  
*In Proc. 11th Eur. Radar Conf.*, 2014, pp. 165–168.
- [31] X. Guo, C. S. Ng, E. de Jong, and A. B. Smits  
Concept of distributed radar system for mini-UAV detection in dense urban environment  
*In Proc. Int. Radar Conf.*, 2019, pp. 1–4.
- [32] A. Huang, P. Sévigny, B. Balaji, and S. Rajan  
Fundamental frequency estimation of HERM lines of drones  
*In Proc. IEEE Int. Radar Conf.*, 2020, pp. 1013–1018.
- [33] D. B. Herr and D. Tahmoush  
Data-Driven STFT for UAV micro-Doppler signature analysis  
*In Proc. IEEE Int. Radar Conf.*, 2020, pp. 1023–1028.
- [34] K. Ren, L. Du, B. Wang, Q. Li, and J. Chen  
Statistical compressive sensing and feature extraction of time-frequency spectrum from narrowband radar  
*IEEE Trans. Aerosp. Electron. Syst.*, vol. 56, no. 1, pp. 326–342, Feb. 2020.
- [35] B. Ozen Bozdag and I. Eerer  
A comparative study on micro-Doppler signature generation methods for UAVs using rotor blade model  
*In Proc. 6th Int. Conf. Electr. Eng.*, 2019, pp. 298–301.
- [36] J. J. M. de Wit, R. I. A. Harmanny, and G. Prémel-Cabic  
Micro-Doppler analysis of small UAVs  
*In Proc. 9th Eur. Radar Conf.*, Amsterdam, 2012, pp. 210–213.
- [37] A. K. Singh, and Y. Kim  
Automatic measurement of blade length and rotation rate of drone using W-Band micro-Doppler radar  
*IEEE Sensors J.*, vol. 18, no. 5, pp. 1895–1902, Mar. 2018.
- [38] Z. Gannon and D. Tahmoush  
Measuring UAV propeller length using micro-Doppler signatures  
*In Proc. IEEE Int. Radar Conf.*, 2020, pp. 1019–1022.
- [39] T. Li, B. Wen, Y. Tian, Z. Li, and S. Wang  
Numerical simulation and experimental analysis of small drone rotor blade polarimetry based on RCS and micro-Doppler signature  
*IEEE Antennas Wireless Propag. Lett.*, vol. 18, no. 1, pp. 187–191, Jan. 2019.
- [40] A. V. Khristenko *et al.*  
Magnitude and spectrum of electromagnetic wave scattered by small quadcopter in X-band  
*IEEE Trans. Antennas Propag.*, vol. 66, no. 4, pp. 1977–1984, Apr. 2018.
- [41] S. Harman  
Analysis of the radar return of micro-UAVs in flight  
*In Proc. IEEE Radar Conf.*, 2017, pp. 1159–1164.
- [42] J. Gong, J. Yan, D. Li, R. Chen, F. Tian, and Z. Yan  
Theoretical and experimental analysis of radar micro-Doppler signature modulated by rotating blades of drones  
*IEEE Antennas Wireless Propag. Lett.*, vol. 19, no. 10, pp. 1659–1663, Oct. 2020.
- [43] K. Marák, T. Pető, S. Bilicz, S. Gyimóthy, and J. Pávó  
Electromagnetic simulation of rotating propeller blades for radar detection purposes  
*IEEE Trans. Magn.*, vol. 54, no. 3, Mar. 2018, Art no. 7203504.

- [44] P. Tait  
*Introduction to Radar Target Recognition, Radar, Sonar, and Navigation*. London, U.K.: Inst. Eng. Technol., 2005.
- [45] M. R. Bell, and R. A. Grubbs  
JEM modeling and measurement for radar target identification  
*IEEE Trans. Aerosp. Electron. Syst.*, vol. 29, no. 1, pp. 73–87, Jan., 1993.
- [46] A. Xiaofeng, Z. Xiaohai, Y. Jianhua, L. Jin, and L. Yongzhen  
Feature extraction of rotating target based on bistatic micro-Doppler analysis  
in *Proc. IEEE CIE Int. Conf. Radar*, 2011, pp. 609–612.
- [47] E. H. Armstrong  
Frequency modulation (FM) tutorial  
[Online]. Available: <https://pdfs.semanticscholar.org/c122/bb065f9a5540970b7a1298a908e88af6dfb9.pdf>
- [48] A. SkyHunter  
[Online]. Available: <https://www.onedrone.com/store/skyhunter-1-800mm-fpv-uav-platform-kit.html>
- [49] DJI Phantom 4 PRO. [Online]. Available: <https://www.dji.com/phantom-4-pro?site=brandsite&from=nav>
- [50] Chase 360. [Online]. Available: [https://www.banggood.com/KDS-Chase-360-V2-6CH-3D-Flying-Flybarless-RC-Helicopter-Kit-p-1510838.html?cur\\_warehouse=CN](https://www.banggood.com/KDS-Chase-360-V2-6CH-3D-Flying-Flybarless-RC-Helicopter-Kit-p-1510838.html?cur_warehouse=CN)
- [51] C. R. Mirabel, M. M. Inacio, and F. Roselena  
Radar cross-section measurement (8–12 GHz) of magnetic and dielectric microwave absorbing thin sheets  
*Revista de Fisica Aplicada e Instrumentacao*, vol. 15, no. 1, 2002, pp. 24–29.
- [52] D. Alexander and Z. Wang  
Nature's flyers: Birds, insects, biomechanics of flight  
*Phys. Today*, vol. 56, 2003, Art. no. 60.
- [53] M. Covell and J. Richardson  
A new, efficient structure for the short-time Fourier transform, with an application in code-division sonar imaging  
In *Proc. Int. Conf. Acoust., Speech, Signal Process.*, 1991, vol. 3, pp. 2041–2044.
- [54] S. Thongkairat, B. Purahong, and V. Chutchavong  
Buffer technique for reduce overlap short time Fourier transform complexity  
In *Proc. Int. Conf. Electron., Inf., Commun.*, 2017, pp. 183–186.



**Byung-Lae Cho** received the B.S. degree in electronic and electrical engineering from Kyungpook National University, Daegu, South Korea, in 1999, and the M.S. and Ph.D. degrees in electronics and electrical engineering from Pohang University of Science and Technology (POSTECH), Pohang, South Korea, in 2001 and 2005, respectively.

Since 2006, he has been a Senior Researcher with the Agency for Defense Development, Daejeon, South Korea. In 2005, he was a Researcher for one year with POSTECH. His research interests include synthetic aperture radar (SAR), interferometric SAR, forward-looking imaging radar, frequency-modulated continuous wave radar, and active electronically scanned array radar.



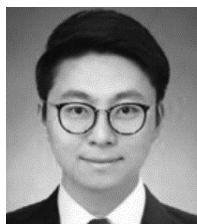
**Jung-Soo Lee** received the B.S. degree in electronic and electrical engineering in 2000 from Chungnam National University, Daejeon, South Korea, and the M.S. degree in electronics and electrical engineering in 2002 from Pohang University of Science and Technology (POSTECH), Pohang, South Korea, where he is currently working toward the Ph.D. degree.

From 2002 to 2005, he was a Researcher with LG electronics, Seoul, South Korea. Since 2006, he has been a Senior Researcher with the Agency for Defense Development, Daejeon, South Korea. His research interests include antenna aperture design, digital signage system, radar system design, and micro-Doppler analysis.



**Kyung-Tae Kim** received the B.S., M.S., and Ph.D. degrees from POSTECH, Pohang, South Korea, in 1994, 1996, and 1999, all in electrical engineering.

From 2002 to 2010, he was a faculty member with the Department of Electronic Engineering, Yeungnam University. Since 2011, he has been with the Department of Electrical Engineering, POSTECH, Pohang, South Korea, and he is currently a Professor. During 2012–2017, he served as the Director of the Sensor Target Recognition Laboratory, sponsored by the Defense Acquisition Program Administration and the Agency for Defense Development. Currently, he is the Director of both the Next Generation Imaging Radar System Research Center, and Next Generation Defense Multidisciplinary Technology Research Center at POSTECH. He is an author of about 300 papers on journals and conference proceedings, and has been the recipient of several outstanding research awards and best paper awards from the Korea Institute of Electromagnetic Engineering and Science (KIEES), and international conferences. He is a member of the IEEE and of the KIEES. He is currently carrying out several research projects funded by Korean government and several industries. His research interests are mainly in the field of intelligent radar system and signal processing: SAR/inverse SAR imaging, target recognition, detection/estimation/tracking, radar resource management, direction of arrival estimation, micro-Doppler analysis, digital beamforming, electronic warfare, and indoor monitoring of individuals.



**Ki-Bong Kang** received the B.S. and M.S. degrees in electronic engineering from Pukyong National University, Busan, South Korea, in 2015 and 2017, respectively. He is currently working toward the Ph.D. degree with the Radar and ElectroMagnetics Signal Processing Laboratory, Pohang University of Science and Technology, Pohang, South Korea.

His current research interests include micro-Doppler analysis, automotive radars, radar signal processing, and inverse synthetic aperture

radar imaging.



**Jae-Ho Choi** received the B.S. degree in computer science and communication engineering from Korea University, Seoul, South Korea, in 2017, and the M.S. degree in electrical engineering from Pohang University of Science and Technology, Pohang, South Korea, where he is currently working toward the Ph.D. degree with the Radar and ElectroMagnetics Signal Processing.

His research interests include radar signal processing, machine learning, and radar application for IoT.